

# Effects of varying field geometry and machine configurations on spatial field traffic intensity: A case study for winter wheat harvest

Katja Augustin<sup>1</sup>  | Santiago Focke Martínez<sup>2</sup> | Rainer Duttmann<sup>1</sup>  |  
Joachim Hertzberg<sup>2,3</sup>  | Michael Kuhwald<sup>1</sup> 

<sup>1</sup>Department of Geography, Christian-Albrechts University, Kiel, Germany

<sup>2</sup>German Research Centre for Artificial Intelligence (DFKI), PBR, Osnabrück, Germany

<sup>3</sup>Department of Computer Science, Osnabrück University, Osnabrück, Germany

## Correspondence

Katja Augustin, Department of Geography, Christian-Albrechts University, Kiel, Germany.  
Email: [augustin@geographie.uni-kiel.de](mailto:augustin@geographie.uni-kiel.de)

## Funding information

Bundesministerium für Bildung und Forschung, Grant/Award Number: 031B0684B and 031B0684C; Ministry of Science and Culture of Lower Saxony; Volkswagen Foundation; Federal Ministry of Education and Research (BMBF)

## Abstract

Increasing traffic intensities in agricultural work processes increase the risk of subsoil compaction. The objective of this study is to investigate whether the geometry of the field and size of the machine influence the traffic intensity. This study focuses on analysing the influence of the machinery and field geometry on the traffic intensities in the field based on wheat harvest operations performed with one combined harvester. For this purpose, 177 routes on 59 different fields are simulated with a route planner, and subsequently, the tracks and traffic intensities are modelled. The structure of the field was specified using eight different shape indices. The analyses showed that the configuration of the machines mainly influences the total passed area and the wheel load distribution on the field. Independent of the machine, the geometry of the field has an influence on the area proportions in the headland with wheel passes above 5 and 10. The indices that highly correlate with traffic intensity are the mean interior edge ratio, the interior area ratio and the mean fractal dimension. It means that the larger the field area in proportion to the perimeter and the infield area, the larger the area fraction with more than 5 or 10 passes. Moreover, this area share increases with the complexity of the field geometry, expressed by the mean fractal dimension. Consequently, the size of the field mainly influences the traffic in the headland because of the removal of the crop.

## KEYWORDS

combine harvester, field geometry, field traffic intensity, soil compaction risk, wheel load, wheel passes

## 1 | INTRODUCTION

The increasing mechanical intensification of cultivation (Keller et al., 2019; Schjønning et al., 2015) represents one

of the major challenges to the preservation of healthy soils in arable land (FAO, 2015).

Soil compaction and especially subsoil compaction is often accompanied by mechanical intensification

This is an open access article under the terms of the [Creative Commons Attribution-NonCommercial](https://creativecommons.org/licenses/by-nc/4.0/) License, which permits use, distribution and reproduction in any medium, provided the original work is properly cited and is not used for commercial purposes.

© 2022 The Authors. *Soil Use and Management* published by John Wiley & Sons Ltd on behalf of British Society of Soil Science.

leading to a loss of soil functions (Destain et al., 2016; Horn et al., 2003), increase of erosivity (Alaoui et al., 2018; Saggau et al., 2019) and decrease of yield (e.g. Arvidsson & Håkansson, 2014; Daigh et al., 2020).

While topsoil compaction may be lowered by primary tillage (Kuhwald et al., 2017, 2020), subsoil compaction (usually >30 cm depth) is usually long-time persistent or very time- and cost-intensive to repair (Chamen et al., 2015; Keller et al., 2017, 2021; Seehusen et al., 2021). How intensively the pressure applied by machines can penetrate into the soil and possibly cause damage depends on several machine features (e.g. tire dimensions, tire inflation pressure and wheel load) and the soil conditions (e.g. soil moisture, soil texture and organic matter) (Gut et al., 2015; Horn et al., 1995; Keller & Arvidsson, 2004; Lamande et al., 2007). In addition to the machine characteristics, the number of wheel passes is also an important factor affecting soil compaction in deeper soil layers. Although measurements show that the first pass causes the greatest soil settlement or pressure input (Horn et al., 2003; Pytka, 2005; Seehusen et al., 2019), multiple wheel passes result in pressure propagation into the depth and thus into the subsoil (Becerra et al., 2010; Botta et al., 2009; Naderi-Boldaji et al., 2018; Pulido-Moncada et al., 2019).

An overall threshold value for wheel passes or wheel load from which subsoil compaction may occur has not been reported yet. Generally, the higher the wheel load, the deeper the pressure penetrates into the soil (Håkansson & Reeder, 1994; Lamande & Schjonning, 2017). However, some studies give indications of critical values, for example, a maximum wheel load of 3 Mg (Horn et al., 2003) or 5 Mg (Becerra et al., 2010; Håkansson & Reeder, 1994; van den Akker et al., 2003). A field experiment by Pulido-Moncada et al. (2019) revealed that the combination of 8-Mg wheel load with 4 wheel passes had a stronger effect in the subsoil than one pass with 12 Mg wheel load.

Moreover, it is still not clear whether it is better to wheel (i) a high area share with less wheel passes and low wheel load or (ii) less area share with more wheel passes and higher wheel loads. Because of the high variation in combined harvester setups, both scenarios are feasible.

At the field scale, high traffic intensities in the field can occur both in terms of wheel loads and wheel passes (Augustin et al., 2020; Bondi et al., 2020; Duttmann et al., 2013; Kroulík et al., 2009). The distribution and quantitative analysis of spatial traffic intensities serve, among other things, to identify hot spots (Augustin et al., 2020; Duttmann et al., 2013) and can assist to optimize traffic management. Most notably, field headlands are affected by high intensities (Augustin et al., 2020) and thus stronger degradation of soil and plant conditions

(Sunoj et al., 2021; Ward et al., 2021). According to Sunoj et al. (2021), targeted and better management of headlands can lead to increased yield in the headland, depending on the field size.

Over the last years, support systems and tools offering generation of routes for machines participating in input-, output- and neutral-material flow operations in arable farming have been developed based on different goals and criteria (Moysiadis et al., 2020; Nilsson & Zhou, 2020). These include both capacitated and noncapacitated scenarios. For example, Bochtis et al. (2012) developed a decision support system (DSS) for route-planning targeting input material flow operations, which aims to reduce the risk of soil compaction. Vahdanjoo et al. (2020) present a tool for track sequence selection aiming to minimize the nonworking distance travelled by the machine in a manure scenario with multiple depots. Edwards et al. (2017) present a route planner for neutral material flow operations aimed to minimize the distance travelled by the machine. Moreover, a spatiotemporally constraint planning method for a harvesting scenario, where harvesters were assisted by a transport vehicle has been presented by Scheuren et al. (2013). Optimizing the routing of, for example, crop harvest with transportation vehicles can already amount to reducing the traffic intensity in the field (Villa-Henriksen et al., 2020). Harvesting processes are one of the most intensive and laborious operations in arable farming, hence route planning that supports such field operations can help optimize the process and mitigate negative effects. In this study, we focus on wheat crops, which represent the highest share of arable land worldwide (about 15.6% in 2019) and one of the most important crops in Europe (FAO, 2021). In mechanized agriculture, wheat is usually harvested using combine harvesters; and there is a high diversity of machine models in the market with widely differing specifications and characteristics. Typically, the dimensions of the available machines vary depending on the manufacturer, the country of sale and the regional farm structures. In Germany, for example, the manufacturer Claas sells harvesters with working widths between 3.7 and 13.8 m and empty weights between 8.9 Mg (Avero 160) and 22.5 Mg (Lexion 8900) (Claas KGaA mbH, 2021). The selection of the machine used for a certain harvesting operation depends, among other factors, on the field size and the total area to be harvested.

A logical assumption is that field geometry influences the efficiency and intensity of traffic as harvesting. Several studies have investigated the influence of field geometry on logistic coefficients both as single-variable (Gonzalez et al., 2004; González et al., 2007; Griffel et al., 2020; Luck et al., 2011) and multivariate analysis (Luck et al., 2011; Oksanen, 2013). It was found that the ratio between the perimeter and the area

of the field (IER) has a significant influence on-time efficiency (Griffel et al., 2020), operational efficiency (Oksanen, 2013) and overlap error (Luck et al., 2011). Griffel et al. (2020) determined that time efficiency for harvesting grass crops improves with increasing IER. Overlap increases with increasing IER in the case of spraying operations according to Luck et al. (2011). Focusing on soil compaction and soil degradation, Duttman et al. (2013) determined that the width-to-length ratio of the field has an impact on the traffic intensity during maize harvests. Thus, an unadjusted length to the loading capacity of the machinery leads to unnecessary passes and increased stress on the soil. However, mainly fields with rectangular field geometries were studied by Duttman et al. (2013). In the case of irregular field geometries, there is no clear length or width of the field, hence the width-to-length ratio is difficult to determine (e.g. for round field shapes).

This study aims to broaden the topic of changing traffic intensity with irregular field shapes. The objective is to analyse and interpret the field traffic intensity for three different combined harvesters on 59 fields with heterogeneous field geometry

1. by modelling the traffic intensity for the three different combined harvesters and
2. by investigating the relationship between the traffic intensity and field geometries by applying eight different shape indices.

To achieve the objective, the spatial traffic intensity of winter wheat harvest was modelled with FiTraM (Augustin et al., 2019) using routes generated by the planning tool presented in Focke Martinez et al. (2021). The operations were planned for a case scenario where only one harvester is in use and unloading the bunker takes place outside the field. The field geometry is characterized by eight field shape indices, which shall reflect the complexity of the shape.

## 2 | METHODS AND MATERIALS

### 2.1 | Study site

A total of 59 fields in the southeast of Schleswig-Holstein, Germany, were selected for field traffic analysis (Figure 1). The region is characterized by intensive agriculture use, with 70% of the area being arable land (Saggau et al., 2019). The field shapes are heterogeneous and dominated by crop rotations with winter wheat (*Triticum aestivum* L.), winter barley (*Hordeum vulgare* L.) and rapeseed (*Brassica napus* L.).

In 2019, the average winter wheat yield in this region was 8.9 Mg ha<sup>-1</sup>, while the 6-year average was at 9.2 Mg ha<sup>-1</sup> (Statistische Ämter des Bundes und der Länder, 2021).

Parent material is glacial till deposited during the Weichselian glaciation. Predominating soil type is Luvisol (WRB, FAO, 2014), while erosion processes form Regosols on the slopes and colluvial deposits in the depressions (Saggau et al., 2019). Soil texture classes vary between loamy sand and sandy loam, with occasional occurrence of sand and loam.

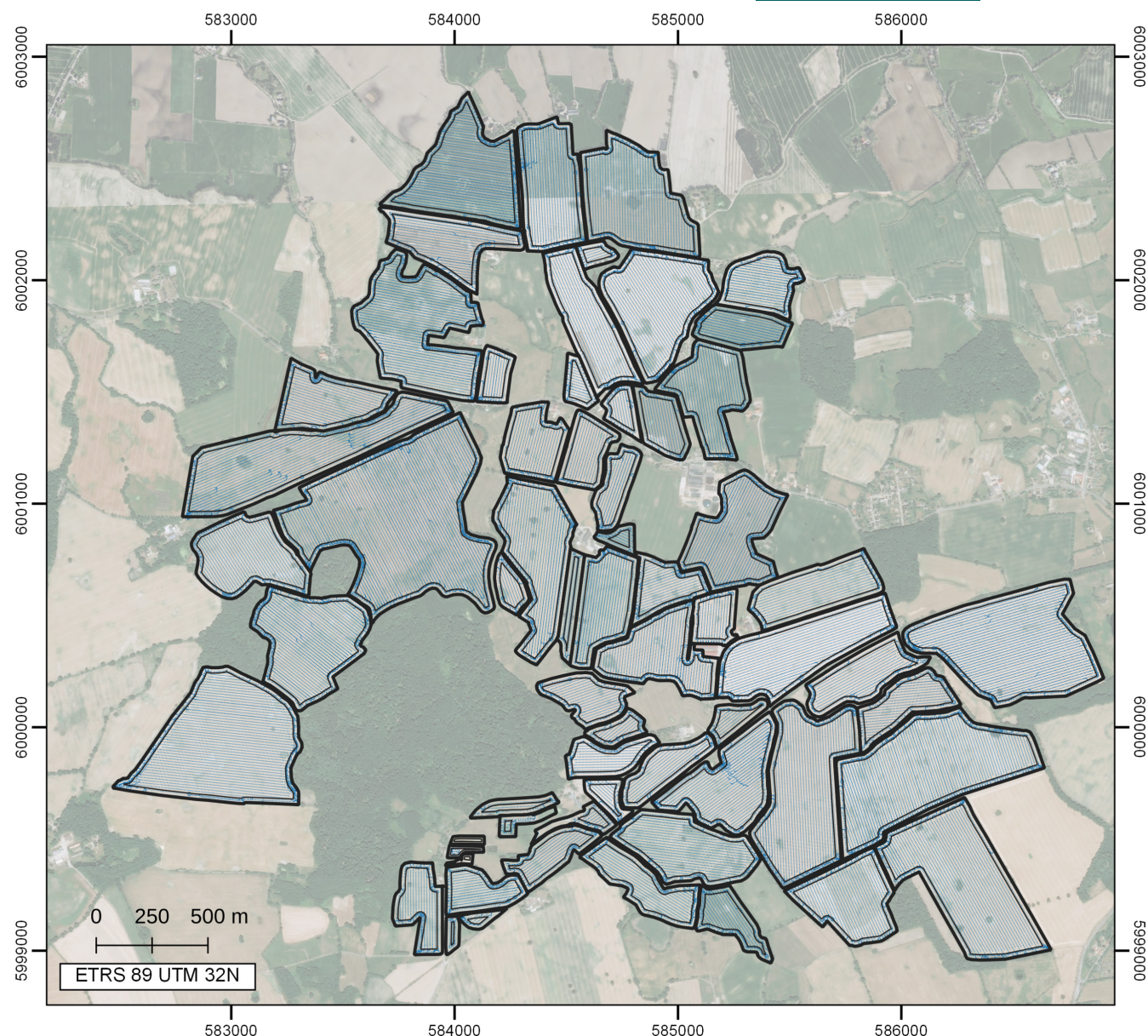
The climate is humid, with mean annual precipitation of 735 mm and a mean temperature of 9.2°C (weather station Doernick, DWD). For winter cereals, soil primary tillage is commonly performed in autumn (September–October), followed by sowing in October. During the growing season, several applications of fertilizer and pesticides take place. The harvest period is, depending on weather conditions, between mid-July and end of August. Harvest is usually executed by combine harvesters, which can store the grains during the harvesting process in a bunker. The bunker is emptied at an unloading point (e.g. an extra transportation vehicle) either in the field or near the field border. For this case study, an unloading point was located outside the field boundary in the vicinity of each field access point. No field obstacles (e.g. trees, ponds, etc.) were taken into account.

### 2.2 | Machine configuration and data preparation

Three different types of combine harvesters were selected for this study, which shall represent a part of the various possibilities of configurations for harvesters. The harvesters' settings were chosen according to consultations with a local farmer and expert in agricultural technology. The machine data were derived from the database of the Advisory Board for Technology and Construction in Agriculture e.V. (KTBL). The three selected combine harvesters (Table 1, S04) differ in mass (15–20.8 Mg), bunker capacity (9500–12,000 L) and working width (6–12 m).

For field traffic intensity analysis, the geometrical properties of the field as a border, headland's position and dimension, and driving direction of each field are considered. The field boundaries and the reference line for the direction of travel were identified and digitalized by visual evaluation from orthophotos (<http://ecn.t3.tiles.virtualearth.net/tiles/>) using QGIS. The headland is defined as the area parallel to the field boundary and includes the turning and the nonturning headland





### Shape Indices for the field Geometries

n = 59	area	peri- meter	IER	SIER	Sph	SIInd	MFD	AE	FD	IAR
minimum	0.9 ha	0.4 km	0.007 m <sup>-1</sup>	4.1	3.6	1.152	1.227	38.3 %	1.973	9.2 %
mean	11.5 ha	1.5 km	0.019 m <sup>-1</sup>	4.7	4.2	1.328	1.227	68.0 %	1.995	59.7 %
maximum	51.6 ha	3.7 km	0.050 m <sup>-1</sup>	6.5	5.7	1.828	1.374	90.3 %	1.999	83.6 %

**FIGURE 1** Study site with 59 fields and maximum, minimum and mean of the shape indices. The shape indices are represented by the mean interior edge ratio (IER), the standardized IER (SIER), the sphericity (Sph), the field shape index (SIInd), the mean fractal dimension (MFD), the fractal dimension (FD), the area envelope (AE) and the interior area ration (IAR)

(Sparkes et al., 1998; Ward et al., 2021). The mean headland width measured from the orthophotos was 24 m, hence this was the headland width set for the route planning of the M225 and M375 machines, which have working width of 6 and 12 m, respectively. However, the

M300 machine has a working width of 9 m, hence an increased headland width of 27 m was set for the route planning of this machine. The area of a field that is not occupied by the headlands is hereafter referred to as the infield.



TABLE 1 Combine harvester modelled in this study

Name	Type (kW)	Working width [m] <sup>a</sup>	Capacity [L]	Weight [Mg]	Ratio [%] <sup>b</sup>	Tire	Inflation pressure [kPa] <sup>c</sup>
M225	225	6	9500	15.0	68	900/60R32	190
					32	600/65R28	120
M300	300	9	10,500	17.1	69.4	1050/50R32	190
					30.6	600/65R28	120
M375	375	12	12,000	20.8	71.4	1050/50R32	260
					28.6	600/65R28	120

<sup>a</sup>Empty weight with cutter.  
<sup>b</sup>Ratio for the weight distribution between front and rear axle.  
<sup>c</sup>Recommended inflation pressure for tires from Michelin with the same tire dimensions, 10 km h<sup>-1</sup> speed and full harvest bunker.

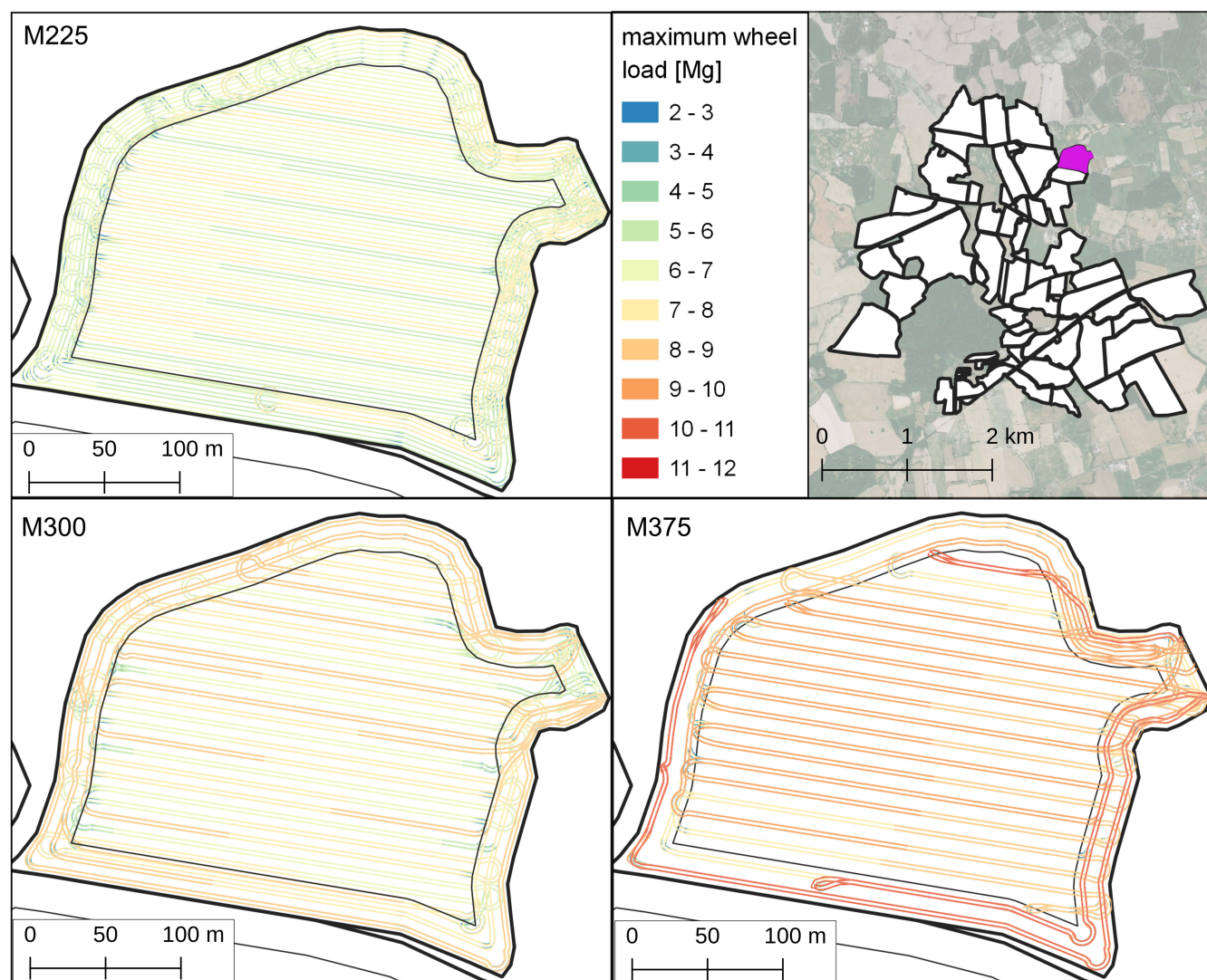


FIGURE 2 Example of field tracks and maximum wheel load for field 1072 used for modelling

### 2.3 | Route planning and modelling of traffic intensity

The route planning tool presented in Focke Martinez et al. (2021) was used to generate the routes of the capacitated wheat harvester. This planner first divides the field

into the surrounding headland and the infield regions based on the desired minimum headland width and generates the tracks for both regions based on the working width of the harvester, the field boundary polygon (for the headland tracks) and a given reference linestring (for the infield tracks). These tracks are to be driven by

the harvester to cover the whole field, starting with the headland tracks (from the outer-most to the inner-most track) followed by the infield tracks (from one side of the field to the other following a basic 'next-adjacent-track' sequence). The process is then divided into working windows based on the average yield mass per area unit in the field (9.2 Mg ha<sup>-1</sup> for this study) and the harvester's bunker capacity. Each working window comprises three operations: (1) harvest the field following the tracks' sequence until the capacity constraint is reached; (2) drive to unloading locations to deposit the harvested yield; and (3) return to the field to continue with the next working window (if needed). For this study, the computation of the working windows was constrained to switch between windows only when a track is completely harvested. For operations (2) and (3), the tool plans the transit paths from/to the unloading location by means of an A\* search on a graph that is generated based on the field geometries (boundaries, tracks, access points, unloading points, etc.). This search is done using a given edge-cost function, which must be defined depending on the desired optimization criteria selected for the operation. In this case, the edge cost is defined by

$$EC = \left\{ \begin{array}{ll} K_p \cdot d \cdot \left( m + 0.2 \cdot \sum m_{prev} \right) & ; \text{edge inside the field} \\ 0.1 \cdot d & ; \text{edge outside the field} \end{array} \right\} \quad (1)$$

where  $d$  is the distance travelled on the edge (in meters),  $m$  is the mass of the machine (in kg) at the moment of planning,  $m_{prev}$  is the sum of machine masses (in kg) corresponding to previously planned edge visits and  $K_p$  is the penalty factor for driving over special edges, defined by

$$K_p = \left\{ \begin{array}{ll} 1 & ; \text{Normal edge} \\ 4 & ; \text{Edge crossing tracks} \\ 11 & ; \text{Edge in the field boundary} \end{array} \right\} \quad (2)$$

The field traffic intensity for the planned routes of the harvester was modeled with FiTraM. A detailed description and evaluation of FiTraM are given by Augustin et al. (2019). FiTraM models the tire tracks for different work processes on the field and derives the spatial information on traffic intensity (number of wheel passes, wheel load and soil stress) as polygons (cf. Augustin et al., 2019, 2020) (cf. Figure 2).

The GPS coordinates and bunker mass information of the route points delivered by the route planner were used as input parameters for FiTraM, together with the machine and tire specifications. A total of 177 processes were

modelled with FiTraM, corresponding to each of the 59 fields with the three different combined harvesters.

The model outputs polygons that represent the tire tracks for every axle on the field (which include information on wheel load) and all tire specifications.

## 2.4 | Traffic intensity analysis and shape indices

After modelling the planned routes with FiTraM, the polygons representing the tire tracks were processed so that overlapping polygons were dissolved. This allows the area percentages of the maximum wheel load to be set in relation to the total area of the field. Additionally, the area percentages of wheel passes were extracted from the raster data (resolution 1 × 1 cm), which was derived from the polygon data by counting the overlapping polygons. The area percentages were calculated for the headland, infield and complete field areas. Contrary to route planning, where headland widths of 24 m (for the M225 and M375 machines) and 27 m (for the M300 machine) were used, the calculation of traffic intensity was done using only a headland width of 24 m. In this study, it was assumed that only the harvester varies, whereas all other working processes remain the same. It was also assumed that the headland is mainly adjusted to the sowing and maintenance tracks. Based on these two assumptions, the headland width of 24 m was not changed for the analysis. Moreover, a headland width of 24 m corresponds to the average tramlines' width in Europe (Gillespie & McDonnell, 2020). Six indices are determined from the modelled tracks (Table 2), which serve to analyse changes in traffic intensity because of varying field geometries. These traffic intensity indices were chosen according to Augustin et al. (2020). The index 5P8L was chosen according to Pulido-Moncada et al. (2019), where it was found that multiple wheel passes of 8 Mg can affect the subsoil.

All indices for traffic intensity were calculated separately for each area's section (infield, headland, complete field) and refer to the percentage of the area of the corresponding section. Concerning LO8, the area percentage corresponds to the area, which was passed at least once with 8 Mg (repeated passes are disregarded). The indicator 5P8L illustrates the combination of wheel load and wheel passes. It represents the area percentage that was passed at least once with 8 Mg and in total at least with five passes. The reason for taking 8 Mg as upper values for the analysis of maximum wheel load is that there would not be any effect of the higher wheel load with a 5 Mg threshold as every machine reaches a load higher than 5 Mg.

To derive the different shapes of field geometries, eight indices were calculated, which shall represent the

**TABLE 2** Shape and traffic intensity indices used for the analysis of field geometry on traffic intensity

Index	Abbreviation	Description
<b>Shape indices</b>		
Area	A	Area of the complete field
Perimeter	P	Perimeter of the field
Mean interior edge ratio	IER SIER	P/A P/sqrt(A)
Standardized IER	Sph	$P/(2 \cdot \sqrt{A})/\pi$
Sphericity	SInd	$P/(2 \cdot \sqrt{A}) \cdot \pi$
Field shape index	MFD	$2 \cdot \log(P)/\log(A)$
Mean fractal dimension	FD AE	See Turci (2016) Field area A divided by envelope area
Fractal dimension	IAR	Ratio between core field area and complete area A
Area envelope interior area ratio		
<b>Traffic intensity</b>		
Load under 8 Mg	LU8	Area-% passed with maximum wheel load $\leq 8$ Mg
Load over 8 Mg	LO8	
Complete area	AP	Area-% passed with maximum wheel load $\geq 8$ Mg
Passes over 5	PO5	
Passes over 10	PO10	Complete area-% passed on the field
Passes 5 to load 8	SP8L	Area-% by $\geq 5$ wheel passes Area-% by $\geq 10$ wheel passes Area passed $\geq 5$ times, at least once with $\geq 8$ Mg

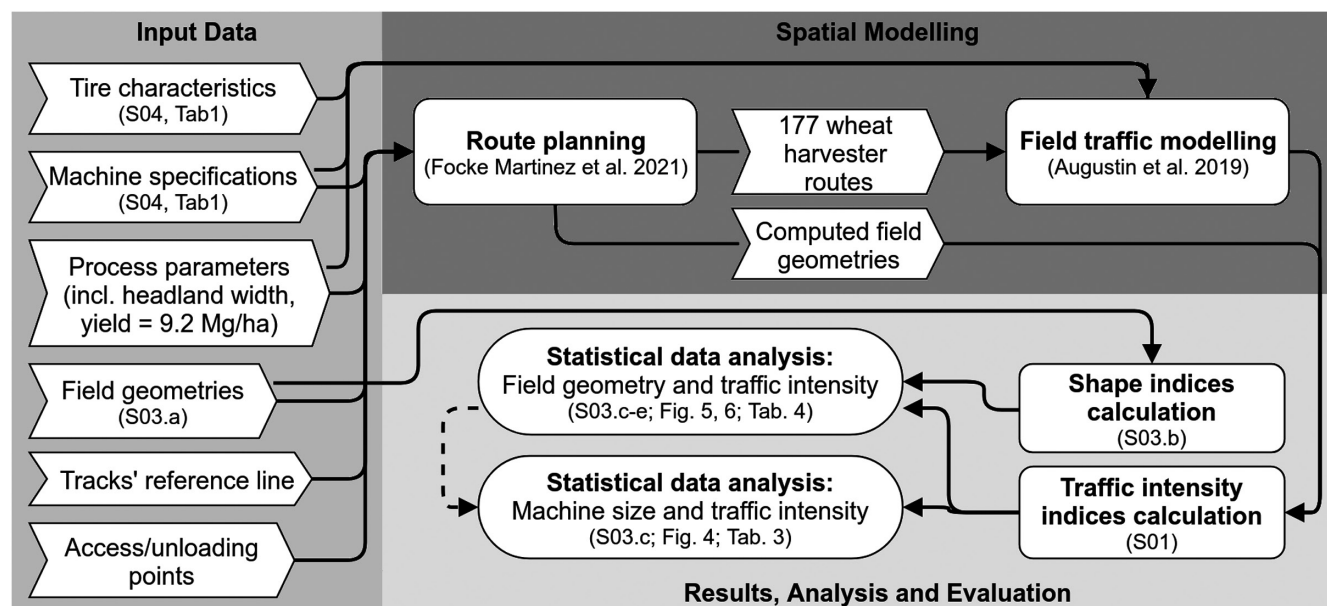


**FIGURE 3** Simplified workflow of the experimental design. The workflow is structured into input data, the spatial modelling part with route planning and tire track/field traffic modelling, and the analysis part with calculations of indices and statistics. The grey text below the processes refers to the tables in the text and supplementary data such as the python scripts

variability in field geometry (Table 2). The indices were taken from Farina (1998); Forman and Godron (1986); Lang and Blaschke (2007); Luck et al. (2011); Oksanen (2013); Schumaker (1996), which were developed for landscape ecology analysis and the determination of field operation efficiency. Most of the indices represent the ratio of area to perimeter and the ratio of

field zone areas. The fractal dimension quantifies the complexity of fractals (Feldman, 2012) and is used to describe the complexity of the field shape. The script for calculating the Hausdorff dimension provided by Turci (2016) was adapted to determine the fractal dimension. The simplified mean fractal dimension (MFD) is a measure of the compactness of the field geometry,



which is defined by the complexity of the field borders. The calculation was adapted from Farina (1998) for an irregular polygon with dimension 2. Table 2 shows the indices used for the spatial geometry and traffic intensity of the field and additionally provides a short description, and the calculation of the shape indices is provided in the supplementary material (S03.a,b).

## 2.5 | Statistical evaluation

Statistics are performed with Python 3.7 and the statistical functions from `scipy.stats` (1.6.1) package.

All tests were applied to all machine combinations, and the samples were differentiated into headland, infield and complete field. All scripts for the hypothesis test and correlation analysis are provided in the supplements (S03.c, S03.d).

The Wilcoxon signed-rank test for paired samples, a nonparametric statistical hypothesis test, was used to determine whether there were differences between the traffic intensity of the different machine configurations. All parameters were tested both two- and one-sided to initially determine whether there were significant differences and subsequently to test whether the distribution of the first observation was larger or smaller than that of the second.

It was also tested whether the distribution varied significantly within the single sample. First, the nonparametric Wilcoxon rank test for one sample was used to check whether the distribution of differences from the mean is symmetric at about zero. Next, the rank correlation by Spearman was applied to calculate the monotone correlation between the geometry indices and traffic intensity.

First attempts were made to determine the equations of correlation for the indices using a regression function (S03.e). This was realized with the Python package `lmfit` (1.0.2).

A simplified overview of the complete workflow is given in Figure 3. It also refers to the input data and scripts provided in the supplementary materials and used during the analysis.

## 3 | RESULTS

### 3.1 | Differences in traffic intensity depending on machine setup

The sizes of the fields ranged from 0.9 ha to 51 ha, with an average of 11.5 ha (Figure 1). The infield covers 9.2% to 83.6% of the total field size. Figure 1 shows the range of the shape indices for the selected fields. It shows that field geometries are very heterogeneous, which is a prerequisite for our analysis to analyse the influence of

geometry on traffic intensities. The (mean) fractal dimension, being dimensionless, is a bit more difficult to interpret in this case the lower the value, the more compact (in case of MFD) and correspondingly more complex the field geometry.

On average for all 59 fields, between 19 and 41% of the total field was passed during the wheat harvest (AP). M225 had the highest mean coverage of the complete field area with 36%. The headland was covered 48% and the infield 32%. The 8-Mg wheel load was never exceeded for M225. M300 covered, on average, 28% of the complete field; 37% of the headland and 26% of the infield. A wheel load of 8 Mg was exceeded for 7.5% of the complete field area and 14.8% of the headland area. M375 had the lowest mean coverage in all area sections, with a coverage of 22% for the complete field area, 30% for headland and 19% for the infield. In total, the AP increases by approx. 7% per 3 m decrease in working width.

In the headland, the average percentage of area that was passed more than five times (PO5) did not exceed 5% for any of the machines. The average area that was passed more than 10 times (PO10) represents <1% (Figure 4). All values are available in the supplements (S01).

The traffic intensities among the three machines differ significantly in almost all traffic intensity indices (Table 3). This is especially true for LO8, LU8 (Figure 4) and AP. The smaller the machine, the higher the passed area and the lower the percentage of areas with more than 8-Mg maximum wheel load (LO8). LO8 was excluded from the analysis of M225 because the machine never reaches an 8-Mg wheel load.

In the infield, M300 had the highest values of PO5 and PO10 compared with M225 and M375, whereas M375 and M300 had higher values than M225 in the headland (Table 3). This means that M375 and M300 pass a larger area fraction more than 10 times in the headland and M300 affects more area in the infield with at least 5 wheel passes. M225 affects less area with high wheel pass frequency, even though M225 passes more area in total than M375 and M300 and, additionally, has to unload the bunker more often because of the lower capacity.

In general, Table 3 and Figure 4 show that the variation in wheel load distributions can be represented by the type and size of the machine, respectively.

There are clear differences in the distributions and mean values of the individual machines, if the values of the wheel load are considered. The PO5 and PO10 indices differ less as a function of machine size, but there is a broader scatter within the distributions of PO5 and PO10. This can be seen, among other things, from the fact that the mean values vary only a little compared with the other machines, but the values for PO5 and PO10 are widely scattered. This indicates that the number of wheel passes is rather determined by an additional coefficient such as geometry.



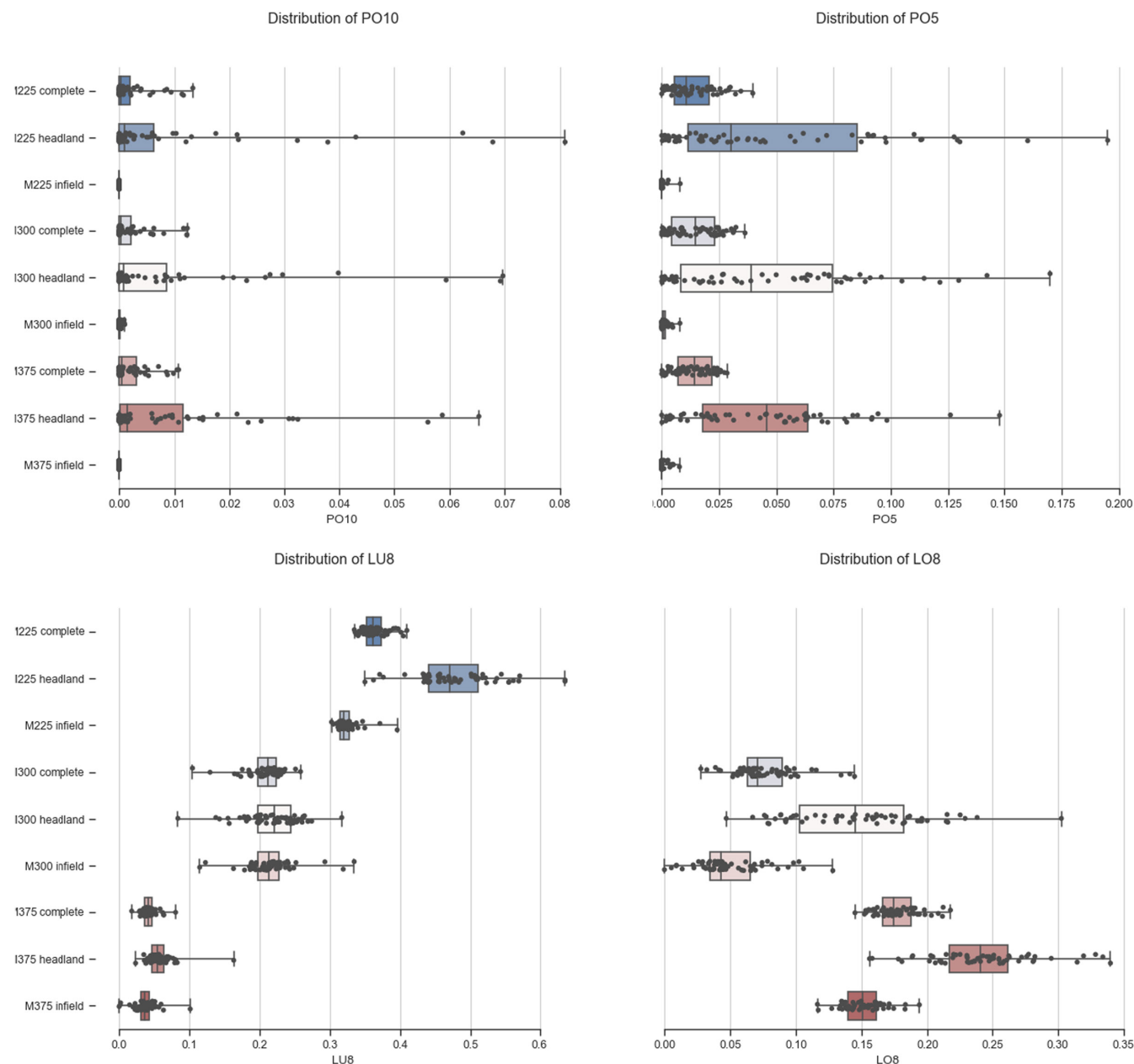


**FIGURE 4** The boxplots for the traffic intensity indices PO5 and PO10 (area share with more than 5 and 10 wheel passes) and LU8 and LO8 (area share with less and more than 8-Mg wheel load) distinguished by the different machines (M225, M300, M375) and field zones (complete field, headland, infield)

For 5P8L, the results only showed relevant differences in the infield between M300 and M375. M300 shows higher area proportions. This is probably because of the higher frequency of passes in the infield.

### 3.2 | Traffic intensities in relation to the field geometry

A wide deviation of the differences from the mean of the distribution within each data set for the traffic intensities means that this index is most likely described or

influenced by at least one other parameter. Table 4 presents the results from the Wilcoxon test for one sample. It shows that there is a significant deviation from the mean of the traffic intensity indices PO5 and PO10, at least in some zones of the field and machines (cf. Figure 4). In the infield, there are also deviations from the mean value for the index 5P8L for both M300 and M375. M225 was disregarded because of the lower wheel load. The only parameter, which is not related to wheel pass frequency, that showed significant deviations from the mean value of the distributions, is the total wheeled area, AP, for M300 in the infield.

**TABLE 3** Wilcoxon rank test for paired samples for the three combined harvesters M225, M300 and M375

				<i>p</i> -Value greater	<i>p</i> -Value less	Significance greater	Significance less
Machines		Zone	Variable				
M300	M225	Complete	AP	–	1.195·10 <sup>−11</sup>	–	**
M300	M225	Complete	LU8	–	1.195·10 <sup>−11</sup>	–	**
M375	M225	Complete	AP	–	1.195·10 <sup>−11</sup>	–	**
M375	M225	Complete	LU8	–	1.195·10 <sup>−11</sup>	–	**
M375	M300	Complete	AP	–	1.258·10 <sup>−11</sup>	–	**
M375	M300	Complete	LU8	–	1.195·10 <sup>−11</sup>	–	**
M375	M300	Complete	LO8	1.195·10 <sup>−11</sup>	–	**	–
M300	M225	Headland	AP	–	1.195·10 <sup>−11</sup>	–	**
M300	M225	Headland	LU8	–	1.195·10 <sup>−11</sup>	–	**
M375	M225	Headland	AP	–	1.195·10 <sup>−11</sup>	–	**
M375	M225	Headland	LU8	–	1.195·10 <sup>−11</sup>	–	**
M375	M300	Headland	AP	–	4.945·10 <sup>−11</sup>	–	**
M375	M300	Headland	LU8	–	1.195·10 <sup>−11</sup>	–	**
M375	M300	Headland	LO8	1.195·10 <sup>−11</sup>	–	**	–
M300	M225	Infield	AP	–	1.626·10 <sup>−11</sup>	–	**
M300	M225	Infield	LU8	–	1.258·10 <sup>−11</sup>	–	**
M300	M225	Infield	PO10	8.717·10 <sup>−7</sup>	–	**	–
M300	M225	Infield	PO5	2.585·10 <sup>−10</sup>	–	**	–
M375	M225	Infield	AP	–	1.195·10 <sup>−11</sup>	–	**
M375	M225	Infield	LU8	–	1.195·10 <sup>−11</sup>	–	**
M375	M300	Infield	AP	–	1.258·10 <sup>−11</sup>	–	**
M375	M300	Infield	LU8	–	1.195·10 <sup>−11</sup>	–	**
M375	M300	Infield	LO8	1.195·10 <sup>−11</sup>	–	**	–
M375	M300	Infield	PO10	–	8.717·10 <sup>−7</sup>	–	**
M375	M300	Infield	PO5	–	1.178·10 <sup>−5</sup>	–	**
M375	M300	Infield	5P8L	–	1.622·10 <sup>−5</sup>	–	**

Note: The table shows whether there are significant differences in field traffic indices between machines and whether the target machine has a lesser or greater distribution than the compared one. The traffic intensity indices are field area shares of the complete area passed (AP), the wheel load under (LU8) and over 8 Mg (LO8), more than 5 (PO5) and 10 (PO10) wheel passes and the area shares for more than 5 passes and 8-Mg wheel load (5P8L). Only the significant results are shown.

Using the results of the Wilcoxon test in Table 4, we see that some traffic intensity indices are influenced by other parameters. So, the Spearman correlation was calculated to analyse which shape indices influence the scattering in the distribution of field traffic intensity. Figure 5 shows the correlation coefficients for the monotonic relationship between the traffic intensity parameters and the field shape indices in the headland. The results for all combinations are shown in the supplements (S02). For completeness, the field traffic indices that were found not to be significant in the previous analysis (Table 4) are also presented in Figure 5.

The results indicate a high monotonic correlation between IAR, MFD and IER with PO5, PO10 and 5P8L in the headland. M225 has no correlation.

coefficients for 5P8L and LO8 as there is no area passed with more than 8 Mg. Considering the complete field area,

the correlation coefficient of the aforementioned variables PO5, PO10 and 5P8L with IAR, MFD and IER becomes smaller (S02). In the infield, no correlation between traffic intensities and field geometry exists for M375 and M225. In contrast, M300 shows high correlations between IER, IAR and PO5, PO10 for the infield.

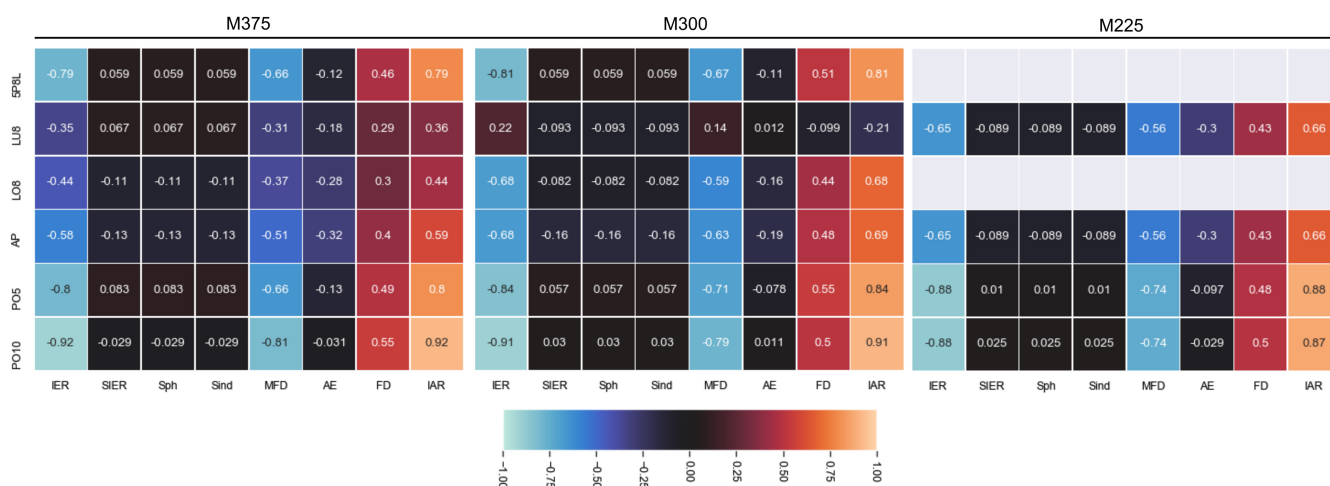
For the headland, the results imply that the areas trafficked for PO5, PO10 and 5P8L increase when the proportion of the headland with respect to the total field area decreases (IAR). These areas decrease, conversely, when the perimeter of the field increases in relation to the field area (IER, Figure 6). They also decrease whether the field geometry becomes more irregular (decreasing MDF).

The dependencies between the traffic intensity indices PO5, PO10 and the shape indices IER, IAR and MFD are presented in Figure 6. Comparing the relationships between these indices, MFD reveals the greatest scatter,

**TABLE 4** Wilcoxon test for one sample that shows the significant deviations of traffic intensity indices of single machines from the mean

Machine	Zone	Variable	Min–Max %	p-Value	Significance
M225	Complete	PO10	(0.0, 0.013)	0.023	**
M300	Complete	PO10	(0.0, 0.012)	0.037	*
M225	Headland	PO10	(0.0, 0.081)	0.0060	**
M300	Headland	PO10	(0.0, 0.070)	0.0212	**
M375	Headland	PO10	(0.0, 0.065)	0.0324	*
M300	Infield	AP	(0.156, 0.400)	0.0431	*
M225	Infield	PO10	(0.0, $1.96 \cdot 10^{-5}$ )	$6.0 \cdot 10^{-7}$	**
M300	Infield	PO10	(0.0, 0.001)	0.0266	*
M375	Infield	PO10	(0.0, $4.49 \cdot 10^{-6}$ )	$1.79 \cdot 10^{-12}$	**
M225	Infield	PO5	(0.0, 0.008)	$1.14 \cdot 10^{-6}$	**
M375	Infield	PO5	(0.0, 0.008)	0.0007	**
M300	Infield	5P8L	(0.0, 0.023)	0.0027	**
M375	Infield	5P8L	(0.0, 0.018)	0.0010	**

Note: The traffic intensity indices are field area proportions of the complete area passed (AP), more than 5 (PO5) and 10 (PO10) wheel passes and the area proportions for more than 5 passes and 8-Mg wheel load (5P8L). Only the significant results are shown. \*, \*\* and \*\*\* indicate the significance level and are clearly assigned to this term in the statistics.

**FIGURE 5** The coefficients of the Spearman correlation between traffic intensity and geometry indices. The traffic intensity indices are field area shares of the complete passed area (AP), the wheel load under (LU8) and over 8 Mg (LO8), more than 5 (PO5) and 10 (PO10) wheel passes, and the area shares for more than 5 passes and 8-Mg wheel load (5P8L). The shape indices are represented by the mean interior edge ratio (IER), the standardized IER (SIER), the sphericity (Sph), the field shape index (Sind), the mean fractal dimension (MFD), the fractal dimension (FD), the area envelope (AE) and the interior area ration (IAR)

while IER shows small deviations. If the individual machines are distinguished in the analysis, the scatter is even higher (S03.e). By using the model functions, limits can be calculated for a given field geometry index to prevent, for example, more than 5% of the area from being passed more than five times. Let us assume that not more than 5% of the area in the headland should be passed more than 5 or 10 times. For the shape index IAR and the traffic intensity index PO5, the value of IAR should not exceed 0.681% (Figure 6). The IAR

value for PO10 is only slightly higher at 0.825%. For IER and PO5, the IER value is 0.014 and for IER and PO10 the 5% threshold is. 0.008. The parameter MFD is transformed back from the logarithmic scale in Figure 6 to the original scale, resulting in an MFD value of 1.265 for PO5 and

1.223 for PO10 for the 5% area share. Generally, for all three geometry indices, a steeper exponential function is seen for PO10 than for PO5, which is why the limit values for the 5% and 10% area share are narrower.



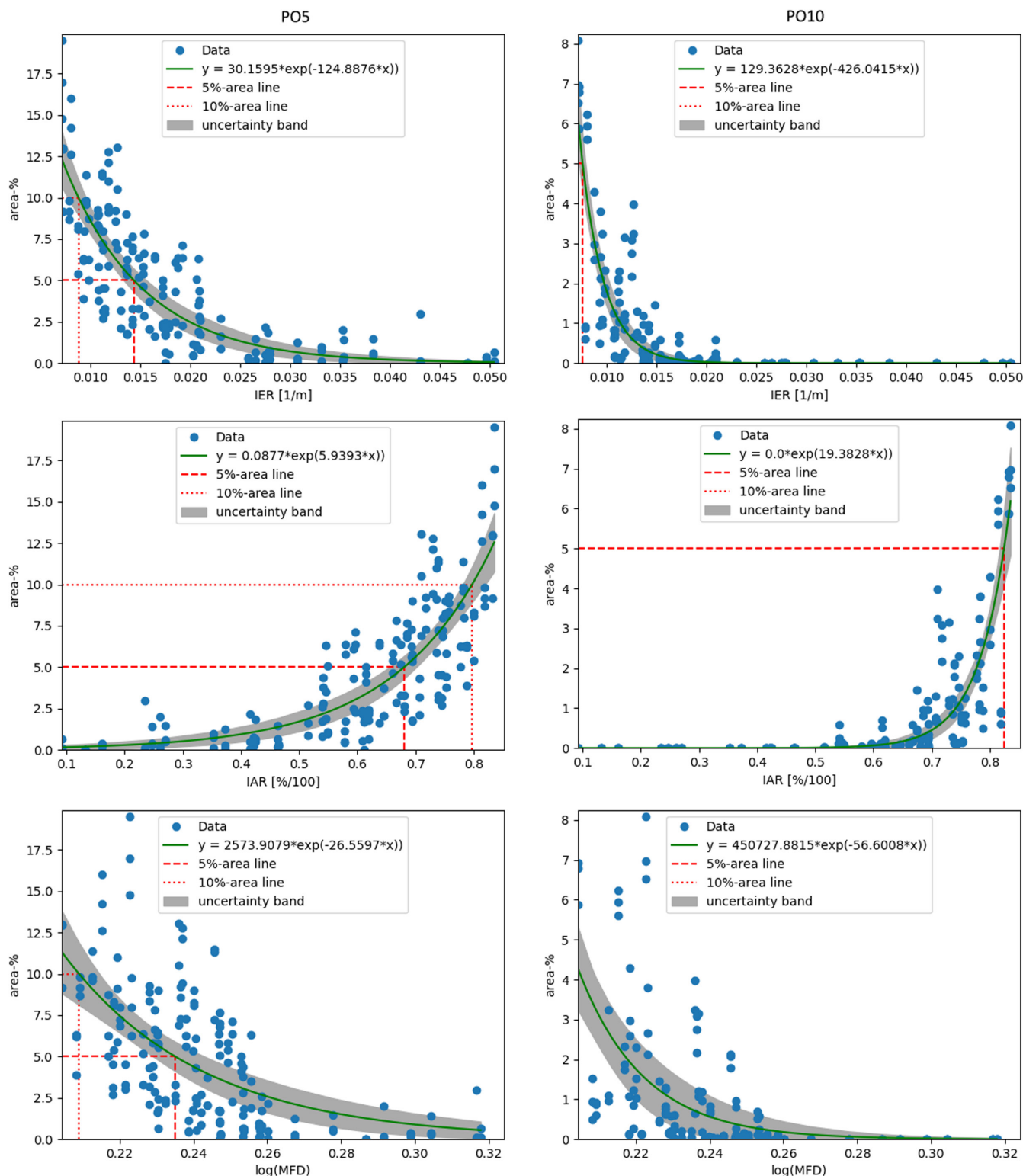


**FIGURE 6** Calculated regression function for the correlation between shape indices and traffic intensity indices for the headland. The traffic intensity indices are the passed area with more than 5 (PO5) and 10 (PO10) wheel passes and the shape indices are the mean interior edge ratio (IER), the interior area ratio (IAR) and the mean fractal dimension (MFD). Plotted with the determined uncertainty of the model function using the lmfit package for Python. Also shown are those lines (in red) at which more than 5% and 10% of the area have been passed with more than 5 or 10 passes. MFD was logarithmized in the figure and in the function to show the function variables at a lower level and thus more clearly

## 4 | DISCUSSION

### 4.1 | The influence of machine type on-field traffic intensity

Both the selection of machines and the field geometry have an influence on the traffic intensity. The influence of the machines is mainly because of the wheel load distribution and the total field area passed, which are defined by the weight and working width characteristics of the machines. Comparing the headland with the infield, the headland shows significantly higher variation within the traffic intensity indices values than the infield. The infield represents the core cultivation area for the crop, which generally shows a lower traffic intensity than the headlands (Augustin et al., 2020; Duttman et al., 2013).

The study shows that the different machines influence other traffic intensity indices than the field geometry indices do. The type of combined harvester mainly determines the wheel load distribution and the total passed area (Figure 4), which seems to be independent of the field geometry. This is reasonable because the passed area declines with the increase in working width. Usually, machines with a larger working width have a higher wheel load, which results in a higher load input on a smaller area. The question of whether to pass (i) a higher area share with lower wheel loads or (ii) a less area proportions with higher wheel loads in practice is hard to answer and also depends on soil texture, soil moisture and other soil parameters (Gut et al., 2015; Lebert & Horn, 1991; Rücknagel et al., 2012).

In the infield, the traffic intensity indices PO10 and PO05 differ between M300 and the other two machines. This is because the headland width during route planning (24m) does not match the width of the headland (27m) during traffic intensity analysis. Multiple wheel passes from the headland thus influence the analysis in the infield traffic from M300. The passed areas at the border between headland and infield within the 24m width are partly added to the infield traffic intensity during the analysis.

The parameter 5P8L shows significant deviations from its mean value in the infield (Table 4). Correlations with the geometry occur mainly in the headland. No significant differences between the machines can be determined for 5P8L either. Since, it can be assumed that 5P8L is mainly defined by the wheel passes, i.e. PO5, and not the load over 8 Mg. In general, the selection of a threshold for wheel load is challenging as high weight differences between the individual machines exist. M225, for example, never reaches the wheel load of 8 Mg. If the threshold value had been set to 5 Mg, as was used by Augustin et al. (2020), M225, M300 and M375 would almost always exceed this value because of wheel loads starting at 5.09 Mg at the front axle (S04). For this reason,

the threshold values were chosen according to Pulido-Moncada et al. (2019) who observed that multiple wheel passes of 8 Mg can have negative effects on the subsoil.

### 4.2 | The influence of field geometry on-field traffic intensity

The analysis revealed that the field geometry has a major effect on the number of wheel passes in the headland. In contrast, the traffic intensity in the infield is less affected by field geometry. More frequent passes are always associated with higher summed wheel loads because each additional pass often leads to an additional pressure input of several Mg. Consequently, with each extra wheel pass, additional pressure is transmitted and propagated into the subsoil and can lead to harmful subsoil compaction (Becerra et al., 2010; Botta et al., 2009; Naderi-Boldaji et al., 2018; Pulido-Moncada et al., 2019).

The IER, IAR and MFD have proven to have a significant effect on traffic intensity indices. Trends in the results show that the smaller the headland is in relation to the infield (IAR) or the shorter the length of the perimeter is relative to the field size (IER), the larger the percentage of area with more than 5 and 10 passes in the headland. The infield shows only minor correlations between wheel pass frequency and field shape as repeated wheeling is usually avoided in the core cultivation area during harvest. However, in practice or with other planning parameters in route planning, the bunker volume may not be adapted to the length or width of the field. In this case, it may be necessary to turn around in the middle of the field in order to drive to the unloading point (cf. Duttman et al., 2013). This is especially the case the larger the field becomes and can lead to a higher number of wheel passes in the infield. The higher correlations for M300 in the infield between the traffic intensity indices PO5, PO10 and the shape indices IER, IAR and MFD are explained in the previous sections. The mean fractal dimension, MFD shows that the area fraction of P05 and P10 increases with increasing complexity (decreasing MFD). The more complex the geometry, the more turning and driving manoeuvres occur on the field, resulting in higher traffic intensities.

Previous studies analysing the influence of field shape on agricultural traffic also showed an influence of the shape indices IER and IAR on different parameters of effective traffic. Luck et al. (2011) found that when the IER becomes larger, the overlap of tracks in spraying application increases. Griffel et al. (2020) revealed that time efficiency during grass crop harvest decreases when area relative to volume increased (decreasing IER). Based on Griffel et al. (2020) and Luck et al. (2011), increasing area

relative to perimeter has a positive effect on both overlap and time efficiency. In contrast, this study reveals a negative effect on traffic intensity by increasing multiple passes when IER decreases. In reflection with the literature, we see that the effect of geometry cannot be applied equally to varying work processes. They should be differentiated both in the parameter investigated to measure the effectiveness or intensity and the work process. In the case studies from Griffel et al. (2020) and Luck et al. (2011), spraying and harvesting with overloading vehicles are working processes where the headland is mostly used for turning the main machine only. In our study, the combine harvester itself carries the threshed wheat from the field to an unloading point outside the field and accordingly has to pass the headland several times. How often this unloading occurs depends on the size of the field. A large headland in relation to the infield size leads to fewer passes from the field and more space in the headland for manoeuvring. Similarly, when the perimeter becomes longer in relation to the total area. Both avoid multiple wheel passes (over 5 and 10 times) in the headland. In future analyses, the headland could be divided into different zones, as was demonstrated by Sparkes et al. (1998); Ward et al. (2021). They distinguished the headland into the turning zone, the transition zone and field edge. This may allow a more accurate traffic intensity analysis within the headland.

To avoid or mitigate high traffic intensities in the headland during winter wheat harvest, the transport routes could be optimized so that a smaller area is covered. For instance, increasing the field access points would reduce the transit distance inside the field. However, the installation of several access points might be restricted by the field characteristics, especially by vegetated or built-up field boundaries, as is often the case in the study area. Another consideration is to keep the area with frequent passes below a certain level and adjust the field size accordingly. For example, fields could be arranged so that the ratio of infield to total field is about 67% to avoid an area more than 5% being passed more than 5 times (cf. Figure 6).

### 4.3 | Modelling, planning assumptions and shape indices

A route planning tool (Focke Martinez et al., 2021) was used to generate approximations of machine trajectories for several field shapes in an automated manner. However, it is important to notice that the traffic analysis was done on routes that were generated following the edge-cost function presented in this paper. Different definitions of this function could result in different machine routes, which would influence the results of the traffic analysis. Additionally, the route planner was set to schedule unload operations

only when the tracks are completely harvested. This setting, together with the used edge-cost function, forces the planner to generate paths avoiding turns inside the infield. Moreover, the route-planning tool is not free of limitations: the machine's turning radius is not considered during the graph-based path planning process, which can result in turns that are impracticable or inadequate for the machine. Furthermore, special turning manoeuvres during harvesting segments are not supported by the planner, for example, when turning while harvesting the headland. Since we did not record the real traffic in this study, the turning manoeuvres cannot be validated for accuracy as was done, for example, with the turning manoeuvres in Augustin et al. (2019). The real travelled tracks and thus traffic intensities can only be reconstructed by modelling the tracks recorded, e.g. by GPS (cf. Augustin et al., 2020; Duttmann et al., 2013; Kroulík et al., 2009; Kroulík et al., 2011).

The shape indices used are mainly based on landscape metrics indicators but are also used in a variety of other research areas where the structure of the geometry matters or is being investigated. In this case, the selection of the shape indices indicates that the harvester's traffic intensity tends to correlate with the geometry indices, which are dependent on the size or perimeter of the field, e.g. the IER or IAR. The indices that describe the shape complexity, e.g. the FD, Sph or the Sind (cf. Table 2), have less influence on the traffic intensity, except for the MFD. In future, other geometry-describing indices could be included to extend the analysis. Thus, also the indices for traffic intensity as, for example, the traffic intensity index by Arvidsson and Håkansson (1991), which is assembled by distance driven and machine weight. The traffic intensity indices represent indicators for the stress on the field and how they differ in terms of machine and field geometry. The selection is derived from given literature. The values and thresholds for traffic intensity analysis are not fixed. In reality, they are dependent on prevailing soil conditions in the field. For example, the moisture at the time of driving and the soil resistance or precompression stress (e.g. Gut et al., 2015; Lebert & Horn, 1991; Rücknagel et al., 2012). However, when planning work processes in the field, it is good to know which conditions (field structure, machine) fundamentally influence the traffic intensity. In this way, unnecessary impact on the field can be avoided in advance.

## 5 | CONCLUSION

The analyses show that both (a) the size of the machine and (b) the geometry of the field structure have a significant influence on the traffic intensity during winter wheat harvest in the field. The machine size mainly influences the parameters of total passed area and wheel load



distribution, while the geometry of the field primarily affects the area with high wheel pass frequencies in the headland. Hence, the larger the area relative to the headland and perimeter, the more often the headland will be passed by a combine harvester to transport the crop off the field. In order to reduce field traffic intensity, the provided regression function may support to identify optimal fractal dimension and infield or perimeter to area ratios to avoid a large share of high traffic intensities in the headland and give indications for potential re-shaping of the field.

The results of this study provide a scientific basis for the area-specific estimation of traffic intensities and, derivatively, soil degradation risks. To our knowledge, previous studies on geometry and traffic intensity are mainly focused on efficient work planning and do not investigate the effects of changing intensities on the field. However, these are worth investigating, especially with regard to the upcoming climatic and social changes, in order to be able to make assessments and forecasts of intensity in agriculture. There have been some studies on the spatial assessment of soil compaction risks (e.g. Kuhwald et al., 2018; 2022). These could be further refined with information on the influence of different geometries and machine configurations.

The results also provide indications of measures to consider in terms of machine configuration and field geometry in order to minimize the intensity of field traffic in practice. The avoidance of high intensities by agricultural traffic is becoming more and more important and represents a wide-ranging challenge in agriculture, as it is nowadays very much focused on effectiveness. Further research should be extended to other work processes and machinery. Those results could contribute to a decision support system (DSS), or part of a DSS, which assists farmers and practitioners in fieldwork planning.




## ACKNOWLEDGEMENTS

The project SOILAssist is funded by the Federal Ministry of Education and Research (BMBF) within the framework of the BonaRes-initiative (grant no. 031B0684C and 031B0684B). The DFKI Niedersachsen Lab (DFKI NI) is sponsored by the Ministry of Science and Culture of Lower Saxony and the VolkswagenStiftung. Open access publishing facilitated by Lincoln University, as part of the Wiley - Lincoln University agreement via the Council of Australian University Librarians.

## DATA AVAILABILITY STATEMENT

Data available on request from the authors.

## ORCID

Katja Augustin  <https://orcid.org/0000-0001-8658-0250>  
 Rainer Duttman  <https://orcid.org/0000-0001-5606-2938>  
 Michael Kuhwald  <https://orcid.org/0000-0003-3346-2888>

## REFERENCES

- Alaoui, A., Rogger, M., Peth, S., & Blöschl, G. (2018). Does soil compaction increase floods? a review. *Journal of Hydrology*, 557, 631–642. <https://doi.org/10.1016/j.jhydrol.2017.12.052>
- Arvidsson, J., & Håkansson, I. (1991). A model for estimating crop yield losses caused by soil compaction. *Soil and Tillage Research*, 20(2), 319–332. [https://doi.org/10.1016/0167-1987\(91\)90046-Z](https://doi.org/10.1016/0167-1987(91)90046-Z)
- Arvidsson, J., & Håkansson, I. (2014). Response of different crops to soil compaction—short-term effects in swedish field experiments. *Soil and Tillage Research*, 138, 56–63. <https://doi.org/10.1016/j.still.2013.12.006>
- Augustin, K., Kuhwald, M., Brunotte, J., & Duttman, R. (2019). Fitram: A model for automated spatial analyses of wheel load, soil stress and wheel pass frequency at field scale. *Biosystems Engineering*, 180, 108–120. <https://doi.org/10.1016/j.biosystemseng.2019.01.019>
- Augustin, K., Kuhwald, M., Brunotte, J., & Duttman, R. (2020). Wheel load and wheel pass frequency as indicators for soil compaction risk: A four-year analysis of traffic intensity at field scale. *Geosciences*, 10(8), 292–307. <https://doi.org/10.3390/geosciences10080292>
- Becerra, A. T., Botta, G. F., Bravo, X. L., Tourn, M., Melcon, F. B., Vazquez, J., Rivero, D., Linares, P., & Nardon, G. (2010). Soil compaction distribution under tractor traffic in almond (*Prunus amigdalus* L.) orchard in almería España. *Soil and Tillage Research*, 107(1), 49–56. <https://doi.org/10.1016/j.still.2010.02.001>
- Bochtis, D. D., Sørensen, C. G., & Green, O. (2012). A dss for planning of soil-sensitive field operations. *Decision Support Systems*, 53(1), 66–75. <https://doi.org/10.1016/j.dss.2011.12.005>
- Bondi, G., O'Sullivan, L., Fenton, O., Creamer, R., Marongiu, I., & Wall, D. P. (2020). Trafficking intensity index for soil compaction management in grasslands. *Soil Use and Management*, 37, 504–518. <https://doi.org/10.1111/sum.12586>
- Botta, G. F., Becerra, A. T., & Tourn, F. B. (2009). Effect of the number of tractor passes on soil rut depth and compaction in two tillage regimes. *Soil and Tillage Research*, 103(2), 381–386. <https://doi.org/10.1016/j.still.2008.12.002>
- Chamen, W. C. T., Moxey, A. P., Towers, W., Balana, B., & Hallett, P. D. (2015). Mitigating arable soil compaction: A review and analysis of available cost and benefit data. *Soil and Tillage Research*, 146, 10–25. <https://doi.org/10.1016/j.still.2014.09.011>
- Claas KGaA mbH. (2021). *Mähdrösch*. Retrieved 11.11.2021, from <https://www.claas.de/produkte/maehdrescher>
- Daigh, A. L. M., DeJong-Hughes, J., & Acharya, U. (2020). Projections of yield losses and economic costs following deep wheel-traffic compaction during the 2019 harvest. *Agricultural & Environmental Letters*, 5(1). <https://doi.org/10.1002/ael2.20013>
- Destain, M. F., Roisin, C., Dalcq, A. S., & Mercatoris, B. C. N. (2016). Effect of wheel traffic on the physical properties of a luvisol. *Geoderma*, 262, 276–284. <https://doi.org/10.1016/j.geoderma.2015.08.028>
- Duttman, R., Brunotte, J., & Bach, M. (2013). Spatial analyses of field traffic intensity and modeling of changes in wheel load and ground contact pressure in individual fields during a silage maize harvest. *Soil and Tillage Research*, 126, 100–111. <https://doi.org/10.1016/j.still.2012.09.001>
- Edwards, G. T., Hinge, J., Skou-Nielsen, N., Villa-Henriksen, A., Sørensen, C. A. G., & Green, O. (2017). Route planning

- evaluation of a prototype optimised infield route planner for neutral material flow agricultural operations. *Biosystems Engineering*, 153, 149–157. <https://doi.org/10.1016/j.biosystemseng.2016.10.007>
- FAO. (2014). World Reference Base for Soil Resources. International Soil Classification System for Naming Soils and Creating Legends for Soil Maps. Rome: World Soil Resources Report 106.
- FAO. (2015). *World reference base for soil resources 2014, update 2015: International soil classification system for naming soils and creating legends for soil maps*. (No. 106). Rome, Italy. <http://www.fao.org/3/i3794en/i3794en.pdf>
- FAO. (2021). *Faostats: Crops and livestock products*. Retrieved 30.09.2021, from <http://www.fao.org/faostat/en/#data/QCL>
- Farina, A. (1998). *Principles and methods in landscape ecology*. Chapman & Hall.
- Feldman, D. P. (2012). *Chaos and fractals: An elementary introduction*. Oxford University Press.
- Focke Martinez, S., Wiemann, T., & Hertzberg, J. (2021). Overview of a route-planning tool for capacitated field processes in arable farming. In A. Meyer-Aurich, M. Gandorfer, C. Hoffmann, C. Weltzien, S. Bellingrath-Kimura, & H. Floto (Eds.), *41. gilljahrestagung, informations- und kommunikationstechnologie in kritischen zeiten* (pp. 97–102). Gesellschaft für Informatik e.V.
- Forman, R., & Godron, M. (1986). *Landscape ecology*. WILEY.
- Gillespie, G. D., & McDonnell, K. P. (2020). Estimating the current area of european tillage systems occupied by tramlines and a potential approach for the cultivation of this underutilised area. *Biosystems Engineering*, 197, 1–11. <https://doi.org/10.1016/j.biosystemseng.2020.06.004>
- Gonzalez, X. P., Alvarez, C. J., & Crecente, R. (2004). Evaluation of land distributions with joint regard to plot size and shape. *Agricultural Systems*, 82(1), 31–43. <https://doi.org/10.1016/j.agsy.2003.10.009>
- Gonzalez, X. P., Marey, M. F., & Álvarez, C. J. (2007). Evaluation of productive rural land patterns with joint regard to the size, shape and dispersion of plots. *Agricultural Systems*, 92(1), 52–62. <https://doi.org/10.1016/j.agsy.2006.02.008>
- Griffel, L. M., Vazhnik, V., Hartley, D. S., Hansen, J. K., & Roni, M. (2020). Agricultural field shape descriptors as predictors of field efficiency for perennial grass harvesting: An empirical proof. *Computers and Electronics in Agriculture*, 168, 105088. <https://doi.org/10.1016/j.compag.2019.105088>
- Gut, S., Chervet, A., Stettler, M., Weisskopf, P., Sturny, W. G., Lamandé, M., Schjønning, P., & Keller, T. (2015). Seasonal dynamics in wheel load-carrying capacity of a loam soil in the swiss plateau. *Soil Use and Management*, 31(1), 132–141. <https://doi.org/10.1111/sum.12148>
- Håkansson, I., & Reeder, R. C. (1994). Subsoil compaction by vehicles with high axle load—extent, persistence and crop response. *Soil and Tillage Research*, 29(2), 277–304. [https://doi.org/10.1016/0167-1987\(94\)90065-5](https://doi.org/10.1016/0167-1987(94)90065-5)
- Horn, R., Domżał, H., Słowińska-Jurkiewicz, A., & van Ouwerkerk, C. (1995). Soil compaction processes and their effects on the structure of arable soils and the environment. *Soil and Tillage Research*, 35(1–2), 23–36. [https://doi.org/10.1016/0167-1987\(95\)00479-C](https://doi.org/10.1016/0167-1987(95)00479-C)
- Horn, R., Way, T., & Rostek, J. (2003). Effect of repeated tractor wheeling on stress/strain properties and consequences on physical properties in structured arable soils. *Soil and Tillage Research*, 73(1–2), 101–106. [https://doi.org/10.1016/S0167-1987\(03\)00103-X](https://doi.org/10.1016/S0167-1987(03)00103-X)
- Keller, T., & Arvidsson, J. (2004). Technical solutions to reduce the risk of subsoil compaction: effects of dual wheels, tandem wheels and tyre inflation pressure on stress propagation in soil. *Soil and Tillage Research*, 79(2), 191–205. <https://doi.org/10.1016/j.still.2004.07.008>
- Keller, T., Colombi, T., Ruiz, S., Manalili, M. P., Rek, J., Stadelmann, V., Wunderli, H., Breitenstein, D., Reiser, R., Oberholzer, H., Schymanski, S., Romero-Ruiz, A., Linde, N., Weisskopf, P., Walter, A., & Or, D. (2017). Long-term soil structure observatory for monitoring post-compaction evolution of soil structure. *Vadose Zone Journal*, 16, 1–16. <https://doi.org/10.2136/vzj2016.11.0118>
- Keller, T., Colombi, T., Ruiz, S., Schymanski, S. J., Weisskopf, P., Koestel, J., Sommer, M., Stadelmann, V., Breitenstein, D., Kirchgessner, N., Walter, A., & Or, D. (2021). Soil structure recovery following compaction: Short-term evolution of soil physical properties in a loamy soil. *Soil Science Society of America Journal*, 85(4), 1002–1020. <https://doi.org/10.1002/saj2.20240>
- Keller, T., Sandin, M., Colombi, T., Horn, R., & Or, D. (2019). Historical increase in agricultural machinery weights enhanced soil stress levels and adversely affected soil functioning. *Soil and Tillage Research*, 194, 104293. <https://doi.org/10.1016/j.still.2019.104293>
- Kroulík, M., Kumhála, F., Hůla, J., & Honzík, I. (2009). The evaluation of agricultural machines field trafficking intensity for different soil tillage technologies. *Soil and Tillage Research*, 105(1), 171–175. <https://doi.org/10.1016/j.still.2009.07.004>
- Kroulík, M., Kvíz, Z., Kumhála, F., Hůla, J., & Loch, T. (2011). Procedures of soil farming allowing reduction of compaction. *Precision Agriculture*, 12(3), 317–333. <https://doi.org/10.1007/s11119-010-9206-1>
- Kuhwald, M., Blaschek, M., Brunotte, J., & Duttman, R. (2017). Comparing soil physical properties from continuous conventional tillage with long-term reduced tillage affected by one-time inversion. *Soil Use and Management*, 33(4), 611–619. <https://doi.org/10.1111/sum.12372>
- Kuhwald, M., Dörnhöfer, K., Oppelt, N., & Duttman, R. (2018). Spatially explicit soil compaction risk assessment of arable soils at regional scale: The sascia-model. *Sustainability*, 10(5), 1618–1629. <https://doi.org/10.3390/su10051618>
- Kuhwald, M., Hamer, W. B., Brunotte, J., & Duttman, R. (2020). Soil penetration resistance after one-time inversion tillage: A spatio-temporal analysis at the field scale. *Land*, 9(12), 482–503. <https://doi.org/10.3390/land9120482>
- Kuhwald, M., Kuhwald, K., & Duttman, R. (2022). Spatio-temporal high-resolution subsoil compaction risk assessment for a 5-years crop rotation at regional scale. *Frontiers in Environmental Science*, 10. <https://doi.org/10.3389/fenvs.2022.823030>
- Lamandé, M., & Schjønning, P. (2017). Soil mechanical stresses in high wheel load agricultural field traffic: a case study. *Soil Research*, 56(2), 129–135. <https://doi.org/10.1071/SR17117>
- Lamandé, M., Schjønning, P., & Tøgersen, F. A. (2007). Mechanical behaviour of an undisturbed soil subjected to loadings: Effects of load and contact area. *Soil and Tillage Research*, 97(1), 91–106. <https://doi.org/10.1016/j.still.2007.09.002>

- Lang, S., & Blaschke, T. (2007). *Landschaftsanalyse mit gis*. Eugen Ulmer.
- Lebert, M., & Horn, R. (1991). A method to predict the mechanical strength of agricultural soils. *Soil and Tillage Research*, 19(2), 275–286. [https://doi.org/10.1016/0167-1987\(91\)90095-F](https://doi.org/10.1016/0167-1987(91)90095-F)
- Luck, J. D., Zandonadi, R. S., & Shearer, S. A. (2011). A case study to evaluate field shape factors for estimating overlap errors with manual and automatic section control. *Transactions of the ASABE*, 54(4), 1237–1243. <https://doi.org/10.13031/2013.39022>
- Moysiadiis, V., Tsolakis, N., Katikaridis, D., Sørensen, C. G., Pearson, S., & Bochtis, D. (2020). Mobile robotics in agricultural operations: A narrative review on planning aspects. *Applied Sciences*, 10(10), 3453–3470. <https://doi.org/10.3390/app10103453>
- Naderi-Boldaji, M., Kazemzadeh, A., Hemmat, A., Rostami, S., & Keller, T. (2018). Changes in soil stress during repeated wheeling: A comparison of measured and simulated values. *Soil Research*, 56(2), 204–214. <https://doi.org/10.1071/SR17093>
- Nilsson, R. S., & Zhou, K. (2020). Decision support tool for operational planning of field operations. *Agronomy*, 10(2), 229–241. <https://doi.org/10.3390/agronomy10020229>
- Oksanen, T. (2013). Shape-describing indices for agricultural field plots and their relationship to operational efficiency. *Computers and Electronics in Agriculture*, 98, 252–259. <https://doi.org/10.1016/j.compag.2013.08.014>
- Pulido-Moncada, M., Munkholm, L. J., & Schjønning, P. (2019). Wheel load, repeated wheeling, and traction effects on subsoil compaction in northern europe. *Soil and Tillage Research*, 186, 300–309. <https://doi.org/10.1016/j.still.2018.11.005>
- Pytka, J. (2005). Effects of repeated rolling of agricultural tractors on soil stress and deformation state in sand and loess. *Soil and Tillage Research*, 82(1), 77–88. <https://doi.org/10.1016/j.still.2004.06.005>
- Rücknagel, J., Christen, O., Hofmann, B., & Ulrich, S. (2012). A simple model to estimate change in precompression stress as a function of water content on the basis of precompression stress at field capacity. *Geoderma*, 177–178, 1–7. <https://doi.org/10.1016/j.geoderma.2012.01.035>
- Saggau, P., Kuhwald, M., & Duttmann, R. (2019). Integrating soil compaction impacts of tramlines into soil erosion modelling: A field-scale approach. *Soil Systems*, 3(3), 51–80. <https://doi.org/10.3390/soilsystems3030051>
- Scheuren, S., Stiene, S., Hartanto, R., Hertzberg, J., & Reinecke, M. (2013). Spatio-temporally constrained planning for cooperative vehicles in a harvesting scenario. *KI-Künstliche Intelligenz*, 27(4), 341–346.
- Schjønning, P., van den Akker, J. J., Keller, T., Greve, M. H., Lalandé, M., Simojoki, A., Stettler, M., Arvidsson, J., & Breuning-Madsen, H. (2015). Driver-pressure- state-impact-response (dpsir) analysis and risk assessment for soil compaction—a european perspective. In D. L. Sparks (Ed.), *Advances in agronomy* (Vol. 133, pp. 183–237). Elsevier Science. <https://doi.org/10.1016/bs.agron.2015.06.001>
- Schumaker, N. H. (1996). Using landscape indices to predict habitat connectivity. *Ecology*, 77(4), 1210–1225. <https://doi.org/10.2307/2265590>
- Seehusen, T., Mordhorst, A., Riggert, R., Fleige, H., Horn, R., & Riley, H. (2021). Subsoil compaction of a clay soil in south-east Norway and its amelioration after 5 years. *International Agrophysics*, 35(2), 145–157. <https://doi.org/10.31545/intagr/135513>
- Seehusen, T., Riggert, R., Fleige, H., Horn, R., & Riley, H. (2019). Soil compaction and stress propagation after different wheeling intensities on a silt soil in south-east Norway. *Acta Agriculturae Scandinavica, Section B — Soil & Plant Science*, 69(4), 343–355. <https://doi.org/10.1080/09064710.2019.1576762>
- Sparkes, D. L., Jaggard, K. W., Ramsden, S. J., & Scott, R. K. (1998). The effect of field margins on the yield of sugar beet and cereal crops. *Annals of Applied Biology*, 132(1), 129–142. <https://doi.org/10.1111/j.1744-7348.1998.tb05190.x>
- Statistische Ämter des Bundes und der Länder. (2021). *Regionaldatenbank deutschland: Erträge ausgewählter landwirtschaftlicher feldfrüchte - jahressumme - regionale tiefe: Kreise und krfr. städteerträge ausgewählter landwirtschaftlicher feldfrüchte - jahressumme - regionale tiefe: Kreise und krfr. städte*. Retrieved 22.06.2021, from <https://www.regionalstatistik.de/genesis/online?operation=table&code=41241>
- Sunoj, S., Kharel, D., Kharel, T., Cho, J., Czymmek, K. J., & Ketterings, Q. M. (2021). Impact of headland area on whole field and farm corn silage and grain yield. *Agronomy Journal*, 113(1), 147–158. <https://doi.org/10.1002/agj2.20489>
- Turci, F. (2016). *Box counting in numpy*. Retrieved 22.06.2021, from <https://francescoturci.net/2016/03/31/box-counting-in-numpy/>
- Vahdanjoo, M., Zhou, K., & Sørensen, C. A. G. (2020). Route planning for agricultural machines with multiple depots: Manure application case study. *Agronomy*, 10(10), 1608–1623. <https://doi.org/10.3390/agronomy10101608>
- van den Akker, J., Arvidsson, J., & Horn, R. (2003). Introduction to the special issue on experiences with the impact and prevention of subsoil compaction in the european union. *Soil and Tillage Research*, 73(1–2), 1–8. [https://doi.org/10.1016/S0167-1987\(03\)00094-1](https://doi.org/10.1016/S0167-1987(03)00094-1)
- Villa-Henriksen, A., Skou-Nielsen, N., Munkholm, L. J., Sørensen, C. A. G., Green, O., & Edwards, G. T. C. (2020). Infield optimized route planning in harvesting operations for risk of soil compaction reduction. *Soil Use and Management*, 37, 810–821. <https://doi.org/10.1111/sum.12654>
- Ward, M., McDonnell, K., Metzger, K., & Forristal, P. D. (2021). The effect of machine traffic zones associated with field headlands on soil structure in a survey of 41 tilled fields in a temperate maritime climate. *Soil and Tillage Research*, 210, 104938. <https://doi.org/10.1016/j.still.2021.104938>

## SUPPORTING INFORMATION

Additional supporting information may be found in the online version of the article at the publisher's website.

**How to cite this article:** Augustin, K., Focke Martínez, S., Duttmann, R., Hertzberg, J., & Kuhwald, M. (2023). Effects of varying field geometry and machine configurations on spatial field traffic intensity: A case study for winter wheat harvest. *Soil Use and Management*, 39, 232–248. <https://doi.org/10.1111/sum.12820>